JOURNAL OF GEOPHYSICAL RESEARCH: SPACE PHYSICS, VOL. 118, 2438–2451, doi:10.1002/jgra.50257, 2013

Non-migrating tides in the ionosphere-thermosphere: In situ versus tropospheric sources

M. Jones Jr.,[1] J. M. Forbes,[1] M. E. Hagan,[2] and A. Maute[2]

Received 27 September 2012; revised 27 February 2013; accepted 29 March 2013; published 10 May 2013.

[1] In this paper we demonstrate how magnetic control of ion-neutral interactions in the ionosphere-thermosphere (IT) system effectively produces source terms for non-migrating solar tides in the neutral momentum equations for the thermosphere. The National Center for Atmospheric Research (NCAR) Thermosphere-Ionosphere-Mesosphere-Electrodynamics General Circulation Model (TIME-GCM) is utilized to quantify these tides, and to assess their importance relative to those that propagate upward from lower atmospheric regions. The primary diurnal tides excited in situ by the above mechanism include DE1, D0 and DW2, with zonal wind amplitudes on the order of 20 m s^{-1} (5–10 m s^{-1}) at ∼500 km (∼350 km) under solar maximum (minimum) conditions. Smaller amplitude semidiurnal non-migrating tides, mainly SE1, S0, SW1, and SW3, are also generated under solar maximum conditions. The aggregate effect of these tidal components is to produce extrema ranging from –110 to +140 m s^{-1} in a typical illustration of latitude versus longitude at a constant local time. The associated wind circulations include vertical wind perturbations that drive temperature perturbations through adiabatic heating and cooling effects. At high latitudes, hydromagnetic coupling effects generate non-migrating tidal components including DE1, D0, DW2, SE1, S0, and SW1, which show interhemispheric differences in both amplitude and latitudinal structure due to interhemispheric differences in the offset between the geographic and geomagnetic poles. Our computational results show that the in situ generated non-migrating tidal components dominate some parts of the tidal spectrum at high levels of solar activity and suggest that in situ generated non-migrating tides must be taken into account in order to reconcile differences in data-model comparisons.

Citation: Jones Jr., M., J. M. Forbes, M. E. Hagan, and A. Maute (2013), Non-migrating tides in the ionosphere-thermosphere: In situ versus tropospheric sources, *J. Geophys. Res. Space Physics*, *118*, 2438–2451, doi:10.1002/jgra.50257.

1. Introduction

[2] The ionosphere-thermosphere (IT) system represents the transition region from Earth's atmosphere to space; thus, furthering our understanding of IT dynamics and electrodynamics is paramount when considering the necessity for more accurate space weather forecasts. During the past decade, and more specifically during the most recent solar minimum period, there has been an upsurge of interest in meteorological influences on IT variability or "space weather". Due to the restrictions imposed by space-based observing platforms, most of the emphasis has been on the longitudinal, seasonal, and interannual variability, which is mainly attributed to global scale perturbations in winds, temperature, and density with subharmonics of a solar day called atmospheric tides. In the context of classical tidal theory [*Chapman and Lindzen*, 1970], solar thermal tides refer to those global-scale oscillations with periods determined by the motion of the Sun relative to the rotating Earth. This formulation requires that these oscillation be *directly* forced by the Sun to be categorized as tides. Other dynamical features that project onto tidal periods and their longitudinal variations, or that vary over intervals shorter than the five to 15 day set-up time for tides [*Vial et al.*, 1991] are known as "pseudo-tides" [e.g., *Walterscheid et al.*, 1986]. Notably, analyses of observational data, or self-consistent atmosphere-ionosphere general circulation simulations cannot distinguish tides from pseudo-tides. Therefore, in this paper we broadly characterize all Fourier components that project onto tidal periods as "tides". In addition to tides excited by thermal sources, our definition encompasses tidal components created by stationary planetary wave-tide [e.g., *Angelats i Coll and Forbes*, 2002] and tide-tide interactions [*Hagan et al.*, 2009], along with in situ thermospheric wind-ion drag interactions that give rise to a spectrum of tidal components. The latter are the foci of this report.

[1]Department of Aerospace Engineering Sciences, University of Colorado Boulder, Boulder, Colorado, USA.
[2]High Altitude Observatory, National Center for Atmospheric Research, Boulder, Colorado, USA.

Corresponding author: M. Jones Jr., Department of Aerospace Engineering Sciences, University of Colorado Boulder, 429 UCB, Boulder, CO 80309, USA. (mcarthur.jonesjr@colorado.edu)

2169-9380/13/10.1002/jgra.50257

[3] In keeping with the above working definition, we now provide the tidal nomenclature to be used throughout the remainder of the present study. We define a tidal oscillation in the atmosphere as

$$A_{n,s}\cos(n\Omega t + s\lambda - \phi_{n,s}) \quad (1)$$

where t = time in UT, Ω = rotation rate of the Earth ($2\pi/24$ h), λ = longitude, n = (1,2,...) is the subharmonic of a solar day, s = (...–3,–2,...0,1,2...) is the zonal wave number and $A_{n,s}$ is the amplitude and $\phi_{n,s}$ is the phase, which are functions of latitude and altitude. In a local time reference frame, expression (1) becomes

$$A_{n,s}\cos(n\Omega t_{\mathrm{LT}} + (s-n)\lambda - \phi_{n,s}) \quad (2)$$

where t_{LT} is local time, since $t_{\mathrm{LT}} = \mathrm{t} + \frac{\lambda}{\Omega}$. The positive integer n = 1, 2, ... corresponds to oscillation periods of 24 h, 12 h, ... and are referred to as diurnal and semidiurnal tides, respectively. In this context, $s > 0$ ($s < 0$) components correspond to westward (eastward) propagating tides. The phase is defined as the time of maximum at 0○ longitude, which is the local time of maximum at Greenwich. When $s = n$ in (2), there is no longitude variability at a fixed local time around a constant latitude circle and these tides are said to be migrating (i.e., Sun-synchronous) because their phase speeds relative to a ground-based observer are all equal to the rotation rate of the Earth, –Ω. When $s \neq n$ and local time is fixed, a given tide with a frequency $n\Omega$ and zonal wave number s has a longitudinal variation of $|s - n|$ (i.e., $|s - n|$ maxima and minima observed in longitude). These waves have zonal phase speeds (C_{ph}) equal to $\frac{-n\Omega}{s}$ and are referred to as non-migrating tides because they do not migrate with the Sun from the perspective of a ground-based observer. Henceforth, we use the notation DWs (SWs) or DEs (SEs) to signify westward or eastward propagating diurnal (semidiurnal) tides, respectively, with zonal wave number s. Standing oscillations (i.e., $s = 0$) are denoted as D0 and S0. Waves with $n = 0$ are referred to as stationary planetary waves (SPW), and with zonal wave number s are denoted as SPWs.

[4] Previous studies aimed at understanding the effects of upward propagating tides on the dynamics and structure of the ionosphere set the stage for the present investigation, in which interactions between the ionospheric plasma and the neutral atmosphere are considered. For instance, *Sagawa et al.* [2005] first observed the wave-4 longitudinal structure in the F-region ionosphere and its seasonal variability, which has been measured in total electron content (TEC) [*Lin et al.*, 2007; *Scherliess et al.*, 2008; *Wan et al.*, 2010; *Pedatella et al.*, 2011] and in situ electron density and temperature measurements [*Lühr et al.*, 2007; *Liu and Watanabe*, 2008; *Pancheva and Mukhtarov*, 2010]. *Immel et al.* [2006] first proposed that the wave-4 signature from near Sun-synchronous orbit in the equatorial ionization anomaly (EIA) is primarily generated by upward propagating tides that modulate the E-region electric fields. More recent numerical studies [*Hagan et al.*, 2007; *Jin et al.*, 2008] also conclude that the four-peaked longitudinal structure in the F-region ionosphere is primarily caused by the modulation of dynamo electric fields in the E-region, due to the upward propagation of non-migrating tides from latent heat release associated with deep tropical convective clouds. Additional studies including *Kil et al.* [2007], *Lühr et al.* [2008], and *Lühr et al.* [2012] all observe the wave-4 longitudinal structure in the $\mathbf{E} \times \mathbf{B}$ drift velocities and equatorial electrojet (EEJ), respectively. Direct propagation of upward propagating tides can also contribute to the longitudinal variability measured in IT quantities, especially those quantities measured at low and middle latitudes [*England et al.*, 2009; *Hagan et al.*, 2009; *England et al.*, 2010]. *Hagan et al.* [2009] shows that SPW4 and SE2 are generated in situ due to the interaction between the DE3 and DW1 and is an important contributor to the wave-4 longitude structure observed in the IT system. Furthermore, *Oberheide et al.* [2011a] suggest that the production of secondary tidal components due to non-linear tide-tide interactions alter the four-peaked structure in the F-region.

[5] Migrating tides generated in the troposphere and stratosphere through the absorption of solar radiation by water vapor (H_2O) and ozone (O_3) propagate vertically into the thermosphere, and have been studied extensively since the 1970s [*Chapman and Lindzen*, 1970; *Forbes and Garrett*, 1979; *Forbes*, 1982; *Hagan*, 1996 and references therein]. In situ generated migrating tides in the thermosphere owe their existence to the absorption of extreme ultraviolet radiation [*Forbes and Garrett*, 1979; *Forbes*, 1982; *Hagan et al.*, 2001 and references therein]. Latent heat release associated with deep tropical convection in the upper troposphere also produces non-migrating tides which propagate vertically into the thermosphere [*Lindzen*, 1978; *Forbes and Garrett*, 1979; *Hagan*, 1996; *Forbes et al.*, 1997; *Oberheide et al.*, 2002; *Hagan and Forbes*, 2002, 2003; *Forbes et al.*, 2006; *Hagan et al.*, 2007; *Oberheide and Forbes*, 2008; *Oberheide et al.*, 2009; *Häusler et al.*, 2010; *Zhang et al.*, 2010a and 2010b]. Specifically, *Oberheide et al.* [2009] found that DE3 attains its maximum amplitude in the upper thermosphere during solar minimum conditions due to reduced molecular dissipation above 120 km. Non-migrating tides are also produced in situ through non-linear tide-tide interactions and non-linear tide-planetary wave interactions [*Teitelbaum et al.*, 1989; *Teitelbaum and Vial*, 1991; *McLandress and Ward*, 1994; *McLandress*, 2001; *Angelats i Coll and Forbes*, 2002; *Mayr et al.*, 2003; *Forbes et al.*, 2008; *Hagan et al.*, 2009]. However, the question still remains, does a longitude dependent ionosphere provide a means for in situ generation of non-migrating tides through ion-neutral coupling? Such a mechanism has been suggested to occur [e.g., *Forbes et al.*, 2009; *Häusler et al.*, 2010; *Oberheide et al.*, 2011b]. In particular, *Oberheide et al.* [2011b] conclude that DW2 and D0 arise from ion-neutral interaction sources in the upper thermosphere.

[6] This paper aims to understand how, and to what extent, longitude variations in the ionosphere, primarily imposed by a realistic magnetic field configuration (i.e., IGRF 2010), introduce complexities in ion-neutral coupling that project onto diurnal and semidiurnal non-migrating tidal components in the neutral atmosphere. For this purpose we employ the National Center for Atmospheric Research (NCAR) Thermosphere-Ionosphere-Mesosphere-Electrodynamics General Circulation Model (TIME-GCM) to perform some numerical experiments that isolate the essential physics. These include simulations that compare results based on the IGRF with those that assume a longitude-independent dipole field aligned with Earth's

rotation axis. In addition we consider how tropospherically generated tides compete with this in situ source by including/excluding tidal forcing based on the Global Scale Wave Model 2009 (GSWM-09) at the lower boundary of the TIME-GCM near 30 km. Spectral decomposition of steady-state September TIME-GCM simulations with the aforementioned magnetic field configurations, in accordance with the inclusion or exclusion of tidal forcing at the model lower boundary, allows us to quantify the non-migrating tidal components generated in situ due to ion-neutral interactions within the IT system. We also examine the relative importance of tidal components at different levels of solar activity. Our results should prove insightful during the upcoming solar maximum period when space-based satellite observations of upper thermospheric longitudinal variability may be partially attributed to the in situ generation of non-migrating tides through ion-neutral coupling processes in addition to vertical propagation of tides from below.

2. TIME-GCM Background and Simulations

[7] The NCAR TIME-GCM is a three-dimensional time-dependent numerical model extending from ∼30 km to ∼600–750 km in altitude (depending on solar cycle) designed to self-consistently calculate the dynamics, photoionization, neutral gas heating, electrodynamics, and chemistry from first-principles in order to replicate the circulation, temperature, electrodynamics, and compositional structure of the mesosphere, thermosphere, and ionosphere. A more complete description of the TIME-GCM is offered by *Hagan et al.* [2009] and references therein, while *Roble and Ridley* [1994], *Roble* [1995, 1996] provide the historical development of the TIME-GCM.

[8] The TIME-GCM simulations in the present study were performed using a horizontal resolution of 2.5° × 2.5° (longitude × latitude), a vertical resolution of 4 points per scale height, and a time step of 120 s. All six TIME-GCM runs were run for the month of September (i.e., day of year 264) until the model reached a diurnally reproducible state. Simulations were performed for solar minimum (solar maximum) conditions using a 10.7 cm solar radio flux (F10.7) value of 75 sfu (10^{-22} W m^{-2} Hz^{-1}) (200 sfu). Geomagnetic proxies representative of quiescent conditions were also held constant in all the simulations using a hemispheric power value [after *Evans*, 1987] of 8 GW, and cross-cap potential drop of 30 kV.

[9] The TIME-GCM intrinsically accounts for atmospheric tides excited due to absorption of ultraviolet and extreme ultraviolet radiation in the stratosphere, mesosphere, and thermosphere. Atmospheric tides or global scale planetary waves with source regions in the troposphere must be introduced as lower boundary conditions. Recent TIME-GCM tidal studies [e.g., *Hagan et al.*, 2009; *England et al.*, 2010; *Häusler et al.*, 2010, *Pedatella et al.*, 2012] have perturbed the TIME-GCM lower boundary (i.e., 10 mb or 30 km) with migrating and non-migrating tidal results from the GSWM [*Hagan et al*, 1995, 1999; *Hagan* 1996], which is a two-dimensional, linearized, steady-state numerical model extending from the surface into the thermosphere. GSWM-02 [*Hagan and Forbes*, 2002, 2003] was recently updated by *Zhang et al*., [2010a, 2010b] to its current version, the GSWM-09. GSWM-09 now includes updated background temperature and wind fields derived from TIMED SABER measurements as well as new radiative and latent heating rates derived from the International Satellite Cloud Climatology Project (ISCPP) and Tropical Rainfall Measuring Mission (TRMM) data, respectively. An intercomparison and assessment of TIME-GCM results that are forced with GSWM-02 and GSWM-09 at the lower boundary is beyond the purview of this report and the subject of a separate study. For the current investigation, we use migrating and non-migrating tides (i.e., DE6 to DW6 and SE6 to SW6) calculated from the GSWM-09 at the TIME-GCM lower boundary for our realistic simulations. Furthermore, the GSWM-09 non-migrating tides introduced at the model lower boundary are the sole source of non-migrating tides not produced in situ and by tide-tide interactions in the TIME-GCM.

[10] In order to frame our work, we provide an overview of the different thermospheric circulations in Figure 1, and make the following definitions. An "idealized" circulation is defined to be a flow that exists in the presence of a dipole magnetic field aligned with Earth's rotation axis and without tidal forcing at the lower boundary. When the dipole magnetic field is replaced by the IGRF field (still without lower boundary tidal forcing), we refer to the corresponding thermospheric circulation as "modified". And finally, when we consider the additional effects of tidal forcing from the GSWM09 imposed at the TIME-GCM lower boundary, we arrive at what we refer to in this paper as the "realistic" thermosphere circulation. Taking into account historical works by *Dickinson and Roble* [1972] and *Roble and Dickinson* [1974], we hypothesize that ion-neutral interactions in the IT system are driven by ionization anomalies due to a longitudinal-dependent ion drag term in the horizontal momentum equations, thus leading to significant differences between the modified and idealized circulations defined above. Similarly, differences between the realistic and modified circulations isolate the effects of tides entering the thermosphere from below.

[11] Figures 1c and 1g show the TIME-GCM realistic flow overlaid on the temperature field on equivalent pressure levels (i.e., $-\ln(p_0/p) = 3.5$) under solar maximum (∼500 km) and solar minimum conditions (∼350 km), respectively. Based on spectral analysis, the dominant zonal wave number for the structures in the temperature and wind fields in Figure 1g is wave-4 under solar minimum conditions, whereas a much smaller wave-4 occurs at solar maximum, and is not identifiable visually in Figure 1c. However, we do note that a wave-4 signature dominates at 100 km at both levels of solar activity (Figures 1d and 1h). This is completely consistent with the differential dissipation that occurs between solar minimum and solar maximum for upward-propagating tides DE3 and SE2, which account for most of the wave-4 structure in the neutral atmosphere [*Oberheide et al.*, 2009]. However, it cannot be discounted that wave-4 plasma structures, originating by dynamo action of these same tides in the ionospheric E-region, could interact collisionally with the neutral atmosphere to produce wave-4 neutral structures as well. This possibility is considered in section 4.

[12] Removing tidal forcing at the TIME-GCM lower boundary (Figures 1b and 1f) causes a clear difference in the longitudinal variability in the temperature field. However, the resulting modified thermospheric circulation

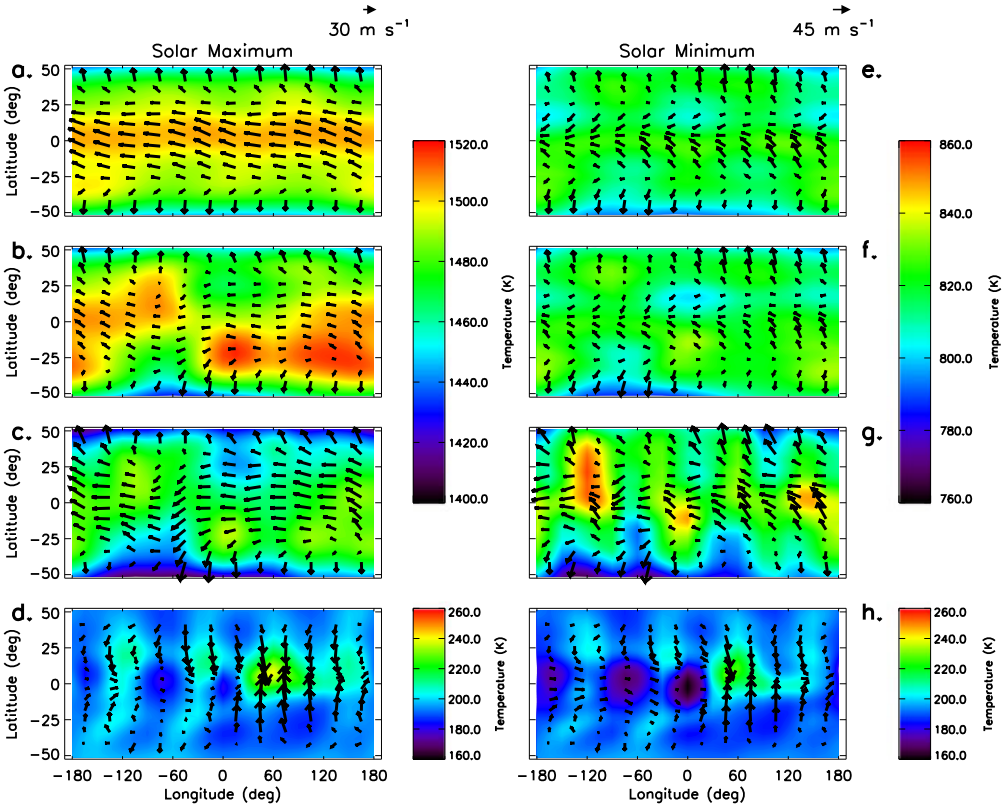

Figure 1. TIME-GCM winds and temperatures at pressure level 3.5 (∼500 km) at 15 LT during September for (a) idealized flow (aligned dipole magnetic field configuration and no GSWM-09 tidal forcing at the lower boundary) during solar maximum, (b) modified flow (realistic magnetic field configuration with no GSWM-09 tidal forcing at the lower boundary) during solar maximum, (c) realistic flow (realistic magnetic field configuration with GSWM-09 tidal forcing at the lower boundary) during solar maximum, and (d) realistic flow at pressure level –6.75 (∼100 km) during solar maximum conditions. (e), (f), and (g) are the same as Figures 1a, 1b, and 1c except for solar minimum conditions at pressure level 3.5 (∼350 km). (h) is the same as Figure 1d except for solar minimum conditions at pressure level –6.75 (∼100 km).

at solar maximum is similar in latitudinal structure and magnitude (Figure 1b) to the realistic circulation observed in Figure 1c, whereas notable differences are seen between these circulations at solar minimum (Figures 1f and 1g). Prescribing an idealized dipole magnetic field and removing tidal forcing at the lower boundary reveals the idealized neutral wind circulation and temperature fields for solar maximum and minimum shown in Figures 1a and 1e. Comparison between the thermospheric temperature and wind fields in Figure 1a with that of Figure 1b clearly show that significant spatial variability in the thermospheric temperature distribution and circulation is introduced in the presence of a longitude-dependent ionosphere at solar maximum. This modified circulation at solar maximum exists due to ion drag source terms in the horizontal momentum equations, which act to perturb the thermospheric circulation from its otherwise idealized motion. As we show below, this perturbation projects significantly onto the D0 and DW2 non-migrating tides as suggested by *Oberheide et al.* [2011b].

[13] The thermospheric temperature and wind fields displayed in Figures 1e and 1f show that under solar minimum conditions, the modified and idealized temperature and winds are nearly identical. We note that the longitudinal variability in the temperature and wind fields at middle latitudes seen in our idealized simulation during solar minimum (Figure 1e) is driven by the combination of longitudinal variability in the high latitude joule heating and the asymmetry of the auroral oval about the geomagnetic poles. This result is counterintuitive to what one would expect for a simulation that has an aligned dipole magnetic field without tidal forcing at the model lower boundary, in which we would expect results to be longitudinally independent. However, this longitudinal variability does not have an affect on the remaining results presented herein.

3. Hydromagnetic Coupling

[14] To aid in interpreting our results, it is useful to think about how the neutral gas is coupled to the ionospheric plasma above about 90 km in Earth's atmosphere. If collision frequencies are sufficiently large between the neutral gas and ionized plasma, then momentum exchange amongst the neutrals and plasma is of potential importance [*Forbes and Garrett*, 1979]. All of the assumptions and approximations used in the mathematical formation of hydromagnetic coupling effects on the neutral gas horizontal momentum equations are discussed in this section; however, the reader is referred to the work of *Richmond* [1971], *Forbes and*

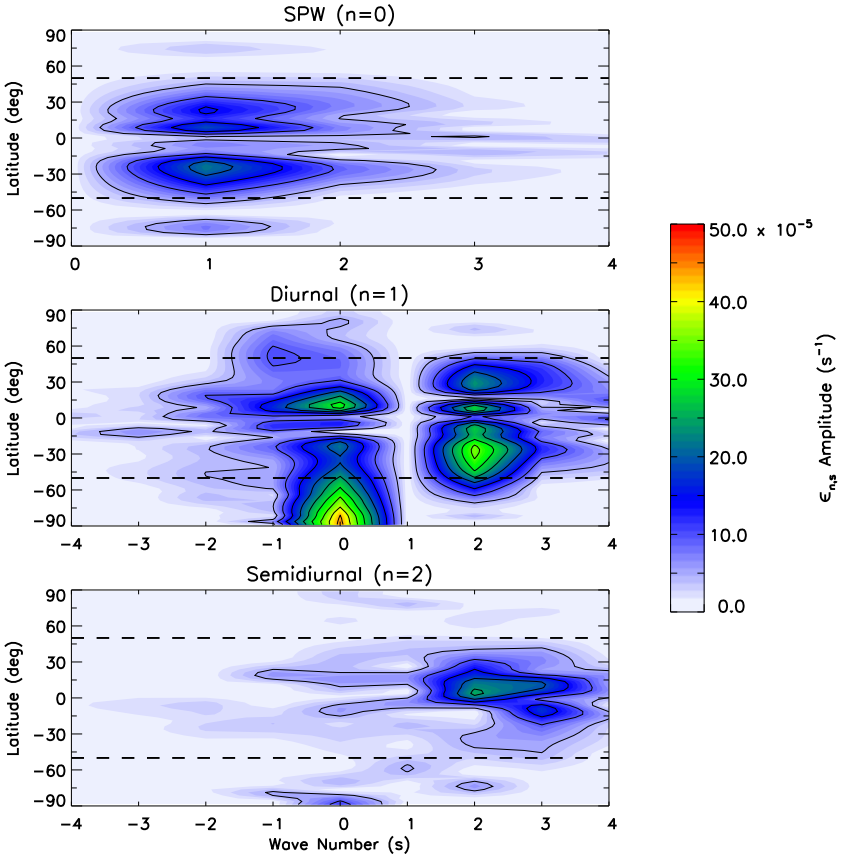

Figure 2. Ion drag components ($\epsilon_{n,s}$) calculated from the TIME-GCM at pressure level 3.5 (∼500 km), during September under solar maximum conditions for the modified flow regime. Components are contoured every 5×10^{-5} $\mathbf{s}^{-1}$. ϵ_0 (zonal mean) and $\epsilon_{1,1}$ (DW1) are set to zero. The dashed lines are at 50°N and 50°S.

Garrett [1979], and references therein for a more complete derivation and description of the methodology used herein.

[15] Hydromagnetic coupling processes affect tidal winds as a result of the Lorentz force in the horizontal momentum equations, which is of the form $(\mathbf{J}\times\mathbf{B})/\rho_0$, where $\mathbf{J}$ is the current density, $\mathbf{B}$ is the magnetic field, and ρ_0 is the background density. Assuming a dipole magnetic field aligned with the Earth's rotation axis, Ohm's law can be written in a simplified form resulting in Lorentz terms following *Richmond* [1971]:

$$[(\mathbf{J}\times\mathbf{B})/\rho_0]_\lambda = -\epsilon_1(u-u^E) + \epsilon_2\cos\theta(v-v^E) \quad (3)$$

$$[(\mathbf{J}\times\mathbf{B})/\rho_0]_\theta = -\epsilon_1(v-v^E) - \epsilon_2\cos\theta(u-u^E) \quad (4)$$

where u (v) is the zonal (meridional) neutral wind, u^E (v^E) is the zonal (meridional) plasma drift, and θ is colatitude. ϵ_1, ϵ_2, and $\mathbf{V^E}$ (plasma drift vector) in (3) and (4) are given by

$$\epsilon_1 = \frac{\sigma_1 B^2(\theta)}{\rho_0}$$

$$\epsilon_2 = \frac{\sigma_2 B(\theta) B_{pole}}{\rho_0}$$

$$\mathbf{V^E} = \frac{\mathbf{E}\times\mathbf{B}}{\mathbf{B^2}}$$

where $\mathbf{E}$ is the electric field, σ_1 and σ_2 are the Pedersen and Hall conductivities, respectively. Additionally, assuming the masses of the neutrals and ions are equal ϵ_1 and ϵ_2 take the form

$$\epsilon_1 \approx \frac{N_i}{N}\frac{\nu_{in}}{1+(\nu_{in}/\omega_i)^2} \quad (5)$$

$$\epsilon_2 \approx \frac{\nu_{in}}{\omega_i}\epsilon_1 \quad (6)$$

where N_i is the ion density, N is the neutral density, ν_{in} is the ion-neutral collision frequency, and ω_i is the ion gyrofrequency.

[16] The terms in (3) and (4) proportional to ϵ_1 are called the "ion drag" force. In the low and middle latitude F-region, the gyrofrequency is much greater than the ion-neutral collision frequency ($\omega_i \gg \nu_{in}$) meaning ions remain "bound" to magnetic field lines. Thus, the neutral gas experiences a loss of momentum when moving across magnetic field lines. This loss of momentum is mainly attributable to zonal momentum exchange due to ion-neutral coupling processes and because the terrestrial magnetic field is tilted in the meridional direction. Terms proportional to ϵ_2 in (3) and (4) are referred to as the "Hall force". Through the collisions of neutrals and ions, the Hall force acts to deflect the wind. *Richmond* [1970] showed that under moderate sunspot conditions the diurnally averaged ion drag force greatly exceeds that of the Hall force above 130 km. Henceforth, we only discuss hydromagnetic coupling effects due to the ion drag force.

[17] Essentially, momentum source terms expressible in terms of non-migrating tidal components arise when

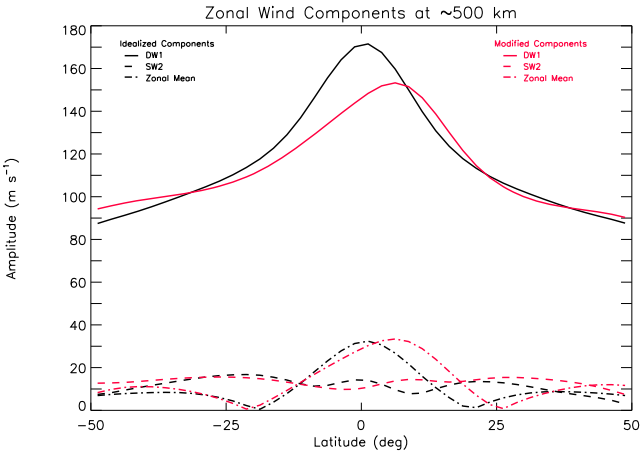

Figure 3. Idealized wind components (black lines) and modified wind components (red lines) calculated from the TIME-GCM at pressure level 3.5 (∼500 km), during September under solar maximum conditions.

considering the nonlinear hydromagnetic coupling terms of the form (ϵu) and (ϵv) in (3) and (4). Our derivations below ignore u^E and v^E, but these terms are included in all computations presented herein. Following the tidal oscillation formulation employed in (1), we now use the exponential form of (1) such that the idealized flow is defined as follows:

$$U_{n,s}\cos(n\Omega t + s\lambda - \phi_{n,s}) = U_{n,s}\frac{e^{i(n\Omega t+s\lambda-\phi_{n,s})} + e^{-i(n\Omega t+s\lambda-\phi_{n,s})}}{2}.$$

After manipulating the complex exponential form of the idealized flow defined above, and considering that the idealized flow in our case is diurnally varying but longitude-independent in the presence of a dipole magnetic field aligned with Earth's rotation axis, we write

$$u \approx u_0 + \sum_{s=n=1}^{2}\left[u^+_{n,s}e^{i(n\Omega t+s\lambda)} + u^-_{n,s}e^{-i(n\Omega t+s\lambda)}\right] \quad (7)$$

where $u^+_{n,s}$ and $u^-_{n,s}$ are the complex amplitudes of the idealized flow. $u^+_{n,s}$ and $u^-_{n,s}$ are given by

$$u^+_{n,s} = \frac{U_{n,s}}{2}e^{i\phi_{n,s}}$$

$$u^-_{n,s} = \frac{U_{n,s}}{2}e^{-i\phi_{n,s}}.$$

The first, second, and third terms in (7) represent the zonal mean zonal wind (u_0), its migrating diurnal ($u_{1,1}$) and migrating semidiurnal ($u_{2,2}$) components, respectively. Latitude variations in all of the above coefficients are implicit. We then ask, what additional momentum source terms appear when a realistic magnetic field is introduced, i.e., when the idealized flow interacts with a longitude-dependent ionosphere ($\epsilon_{n,s}$)? $\epsilon_{n,s}$ takes the following form:

$$\epsilon \approx \epsilon_0 + \sum_{n=0}^{2}\sum_{s=-M}^{M}\left[\epsilon^+_{n,s}e^{i(n\Omega t+s\lambda)} + \epsilon^-_{n,s}e^{-i(n\Omega t+s\lambda)}\right] \quad (8)$$

where M is equal to the zonal wave numbers of appreciable ion drag amplitude. For illustration purposes, let us assume that to first order the more realistic ionosphere now possesses an additional longitude dependence expressible as the zonal mean and SPW1 (i.e., $\epsilon_0 + \epsilon^+_{0,1}e^{i\lambda} + \epsilon^-_{0,1}e^{-i\lambda}$), in other words a wave-1 dependence in longitude. Specifically, we use this form for the realistic ionosphere because

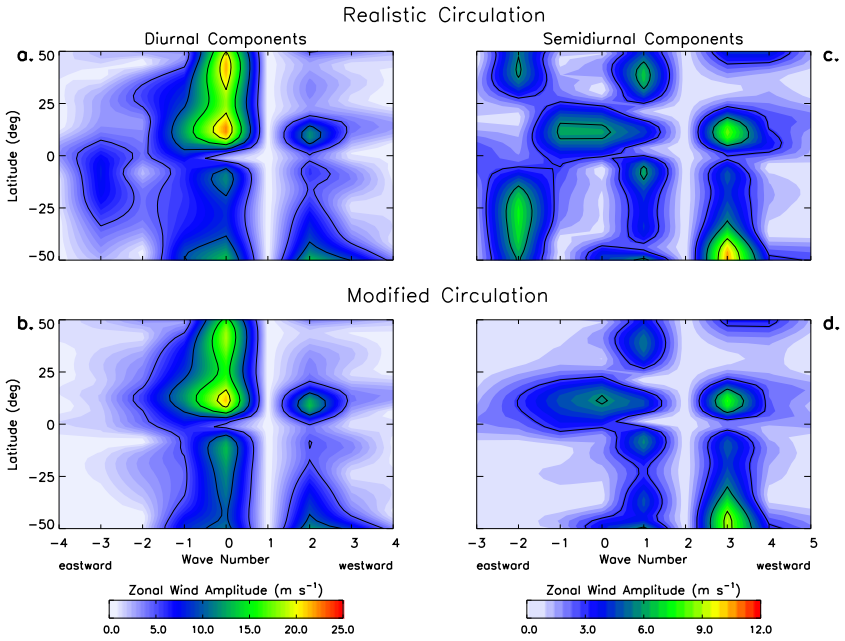

Figure 4. Zonal wind wave number spectra of the diurnal and semidiurnal non-migrating tidal components from the TIME-GCM at pressure level 3.5 (∼500 km), during September solar maximum conditions; (a) and (c) simulating the realistic flow regime; (b) and (d) simulating the modified flow regime. Diurnal (Semidiurnal) components are contoured every 5 (3) m s^{-1}. The migrating tidal amplitudes have been set to zero.

Table 1. Hydromagnetic Coupling Momentum Source Terms[a]

	ϵ_0	SPW1	SPW2	DE1	D0	DW1	DW2	DW3	SW2	SW3
u_0	mean term	SPW1*	SPW2*	DE1*	D0*	DW1*	DW2*	DW3*	SW2*	SW3*
DW1	DW1*	D0,DW2	DE1,DW3	SPW2,S0	SPW1,SW1	mean term,SW2	SPW1,SW3	SPW2,DW4	DW1,...	DW2,...
SW2	SW2*	SW1,SW3	S0,SW4	DW3,...	DW2,...	DW1,...	D0,...	DE1,...	mean term,...	SPW1,...

[a] Hydromagnetic coupling momentum source terms due to the idealized wind circulation and modified ionosphere following the hydromagnetic coupling expansion given in (7) and (8).The top row lists the largest ion drag terms ($\epsilon_{n,s}$) from the modified ionosphere shown in Figure 2. The first column lists the largest zonal wind terms from the idealized wind circulation ($u_{n,s}$) shown in Figure 3. The corresponding momentum source terms for the modified circulation consist of the sum and difference products of $\epsilon_{n,s}$ and $u_{n,s}$, which populate the table. Terms with asterisk represent terms that are modified by the zonal mean quantities. Sum or difference products with $n \geq 3$ are represented by an ellipsis.

the geographic/geomagnetic offset is primarily a wave-1 longitude structure and so SPW1 is important. The product of this term with the zonal mean and DW1 (i.e., $u_0 + u^+_{1,1}e^{i(\Omega t+\lambda)} + u^-_{1,1}e^{-i(\Omega t+\lambda)}$) yields the following source terms in the momentum equation:

$$\begin{aligned}\epsilon u \approx{}& \epsilon^+_{0,1}u_0e^{i\lambda} + \epsilon^-_{0,1}u_0e^{-i\lambda} && \text{(SPW1 terms)}\\ &+ \epsilon^+_{0,1}u^+_{1,1}e^{i(\sigma t+0\lambda)} + \epsilon^-_{0,1}u^-_{1,1}e^{-i(\sigma t+0\lambda)} && \text{(D0 terms)}\\ &+ \epsilon^-_{0,1}u^+_{1,1}e^{i(\sigma t+2\lambda)} + \epsilon^+_{0,1}u^-_{1,1}e^{-i(\sigma t+2\lambda)} && \text{(DW2 terms)}\end{aligned}$$

Thus, we expect that the modified circulation will be strongly characterized by SPW1, D0, and DW2. Of course, additional terms in the expansions for u and ϵ will lead to source terms for additional non-migrating tidal components that constitute the thermospheric circulation modified by the more realistic magnetic field.

[18] Figure 2 shows that the largest amplitude components of the ion drag terms calculated at solar maximum for the modified ionosphere are the SPW1 ($\epsilon_{0,1}$), SPW2 ($\epsilon_{0,2}$), D0 ($\epsilon_{1,0}$), DW2 ($\epsilon_{1,2}$), DW3 ($\epsilon_{1,3}$), and SW2 ($\epsilon_{2,2}$). The zonal mean (ϵ_0) and DW1 ($\epsilon_{1,1}$) are an order of magnitude larger than the other ion drag terms shown in Figure 2 and are therefore set to zero in Figure 2 in order to highlight the other ion drag terms of importance in our hydromagnetic coupling expansion. The zonal mean (u_0), DW1 ($u_{1,1}$), and SW2 ($u_{2,2}$) are the largest components from the idealized neutral wind circulation at solar maximum, and these are shown in Figure 3 (black lines). The more complete set of hydromagnetic coupling terms from above leads to slight modification of the important idealized zonal wind components (Figure 3, red lines). Zonal momentum from the DW1 is transferred into the zonal mean and SW2 components, leading to the creation of non-migrating tidal components (Figure 4b and 4d). Table 1 displays the results of a hydromagnetic coupling expansion that uses all the important terms (i.e., those $\epsilon_{n,s}$ values with amplitudes greater than or equal to 2×10^{-4} s^{-1}) from the modified ionosphere and idealized circulation listed above. For example, Table 1 shows that hydromagnetic coupling between the DW2 component of the modified ion drag ($\epsilon_{1,2}$) and the DW1 ($u_{1,1}$) component of the idealized wind circulation results in a modified wind circulation characterized by SPW1 and SW3 momentum source terms.

[19] Figure 4 depicts the zonal wind wave spectra at pressure level 3.5 (∼500 km) from the modified and realistic simulations under solar maximum conditions at low and middle latitudes. The migrating tides in both Figures 4 and 5 are set to zero to accentuate the non-migrating diurnal

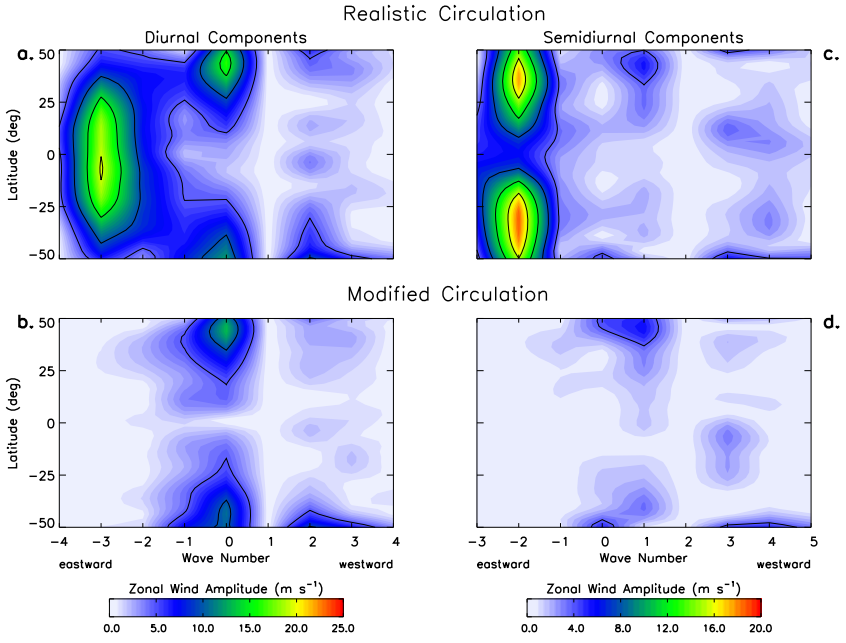

Figure 5. Same as Figure 4 at equivalent pressure level 3.5 (∼350 km) for solar minimum conditions. Diurnal (Semidiurnal) components are contoured every 5 (4) m s^{-1}.

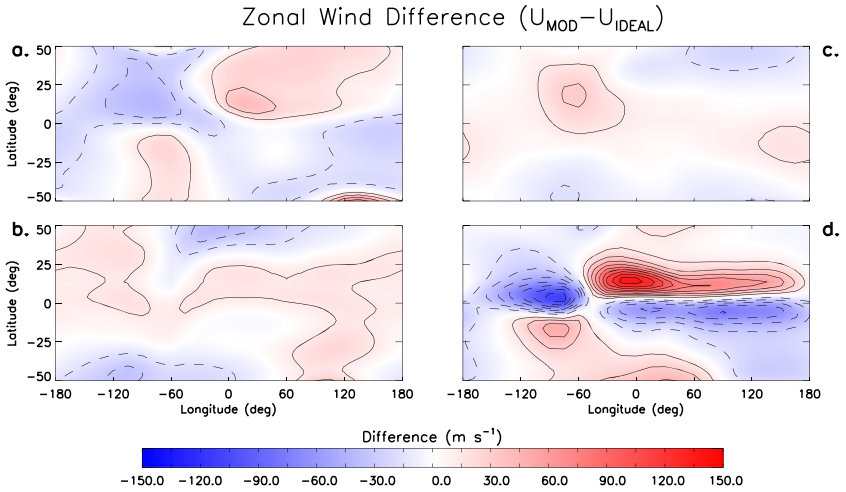

Figure 6. Zonal wind differences between the modified and idealized circulations at pressure level 3.5 (∼500 km) during September under solar maximum conditions at (a) 2 LT, (b) 8 LT, (c) 14 LT, and (d) 20 LT contoured every ±15 m s^{-1}.

and semidiurnal tides generally of smaller amplitude. As expected, the largest diurnal components in the modified circulation are D0 and DW2 which attain amplitudes up to 20 m s^{-1} (Figure 4b). These two non-migrating tides come from the interaction between SPW1 and DW1 (as was shown in the initial simplified hydromagnetic coupling expansion). Therefore, D0 and DW2 are generated in situ in the upper thermosphere due to the non-dipole nature of the geomagnetic field, supporting the conclusion made in *Oberheide et al.* [2011b]. Also, interaction between SPW2 and DW1 leads to a relatively large DE1 (∼ 15 m s^{-1}) zonal wind component at ∼500 km. Coupling between SPW1 and SW2 produces the largest semidiurnal zonal wind components (i.e., SW1 and SW3) in the modified circulation, shown in Figure 4d. Amplitudes of SW1 and SW3 range from 3 to 10 m s^{-1}. The smaller S0 and SE1 (amplitudes ranging from 1 to 7 m s^{-1}) components come from coupling between the SPW2 with SW2 and SPW3 with SW2, respectively.

[20] Figure 4 also shows that at pressure level 3.5 (∼500 km), the diurnal and semidiurnal non-migrating tides are mainly generated in situ due to ion drag at solar maximum. This can be inferred from the evident similarities in latitudinal structure and amplitude between the above non-migrating tidal components calculated for the realistic (Figures 4a and 4c) and modified (Figures 4b and 4d) flow regimes, respectively. Another interesting feature in Figure 4 is the latitudinal asymmetries of the non-migrating tides produced via ion-neutral interactions. These latitudinal differences in tidal amplitude are due to the hemispheric asymmetries in the modified ion drag term (Figure 2), as the ionization anomalies that govern ion-neutral interactions are not only longitudinally dependent, but latitudinal dependent as well. Thus, the resulting momentum source terms shown in Figure 4 are latitudinally asymmetric because they are generated from the products of the modified (i.e., longitude/latitude dependent) ion drag terms with the idealized wind circulation (following Table 1). Other non-migrating tidal components shown in Figures 4a and 4c include DE3 and SE2. Comparison between the realistic circulation and with the modified circulation shows that these tides are of tropospheric origin and are not generated in situ due to ion-neutral interactions. During solar minimum at pressure level 3.5 (∼350 km) (Figure 5), the dominant diurnal and semidiurnal non-migrating tides present are of tropospheric origin (i.e., DE3 and SE2) and there are few similarities in the

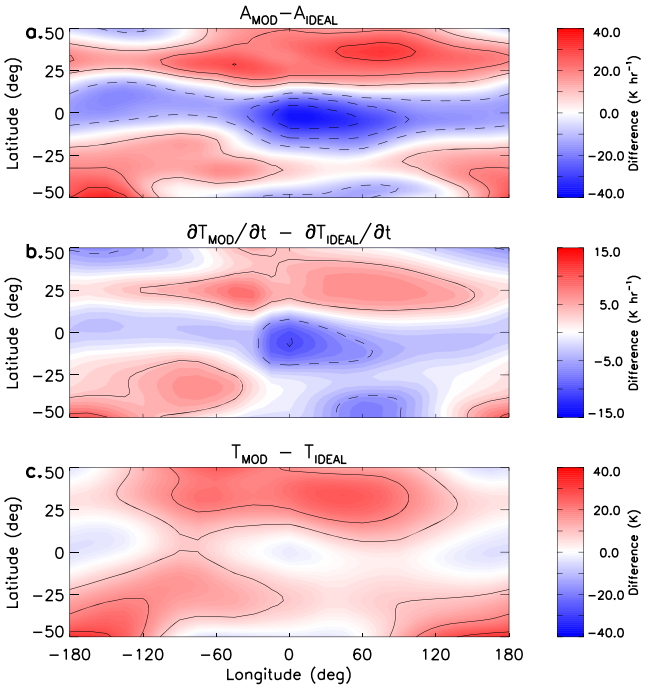

Figure 7. (a) Adiabatic heating differences between the modified and idealized circulations at pressure level 3.5 (∼500 km) during September under solar maximum conditions at 3 LT contoured every 10 K h^{-1}. (b) same as Figure 7a for time of temperature differences contoured every 5 K h^{-1}. (c) same as Figure 7a for temperature differences at 5 LT contoured every 10 K.

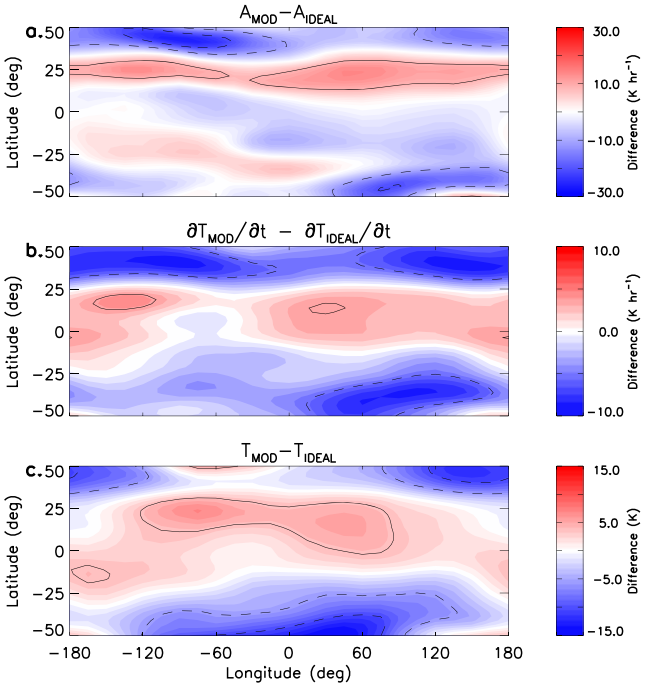

Figure 8. Same as Figure 7 at equivalent pressure level 3.5 (∼350 km) for solar minimum conditions. (a) Contoured every 10 K h^{-1}, (b) contoured every 5 K h^{-1}, and (c) contoured every 5 K.

modified (Figure 5b and 5d) and realistic (Figure 5a and 5c) flow regimes at low to mid-latitudes. Therefore, the in situ ion-drag source of non-migrating tides in the upper thermosphere is of utmost importance during solar maximum, and upward propagating non-migrating tides of tropospheric origin are dominant at low-latitudes at solar minimum, as was concluded in *Oberheide et al.* [2009].

[21] We also consider the results shown in Figures 4 and 5 in light of tidal diagnostics from the CHAMP (CHAllenging Minisatellite Payload) satellite presented in recent works by *Häusler and Lühr* [2009] and *Häusler et al.* [2010]. *Häusler and Lühr* [2009] conclude that along the geomagnetic equator D0, DW2, SW1 and SW3 all significantly contribute to the observed wave-1 longitudinal structure at ∼400 km in the zonal wind field. Figure 4 shows that our TIME-GCM simulations under solar maximum conditions are largely consistent with the above conclusion as the largest amplitude non-migrating diurnal and semidiurnal tidal components in the zonal wind field are D0, DE1, DW2, SW1, and SW3 at ∼500 km and that these non-migrating tides are a result of using a realistic geomagnetic main field approximation. Further comparison between our TIME-GCM results with CHAMP data displayed in *Häusler et al.* [2010] clearly shows that the TIME-GCM can correctly produce the solar cycle dependency observed in the tidal spectrum at ∼400 km. For example, at low and middle latitudes, Figures 4 and 5 show an increase (decrease) in the D0 and DW2 (DE2 and DE3) amplitudes with increasing (decreasing) solar flux, which is consistent with CHAMP observations shown in Figure 3 of *Häusler et al.* [2010]. The amplitudes of the above tidal components are moreover of similar magnitude (e.g., 5 to 12 m s^{-1}) in the TIME-GCM and CHAMP observations.

4. Spatial Variability Introduced by a Realistic Magnetic Field

[22] As we saw in Section 3, non-migrating tides in the horizontal wind fields are excited in the presence of a longitudinally dependent ionosphere associated with a realistic magnetic field configuration (i.e., modified case). The combined effects of these non-migrating tides are substantial at low and middle latitudes, leading to significant spatial variability in horizontal winds. Figure 6 depicts the

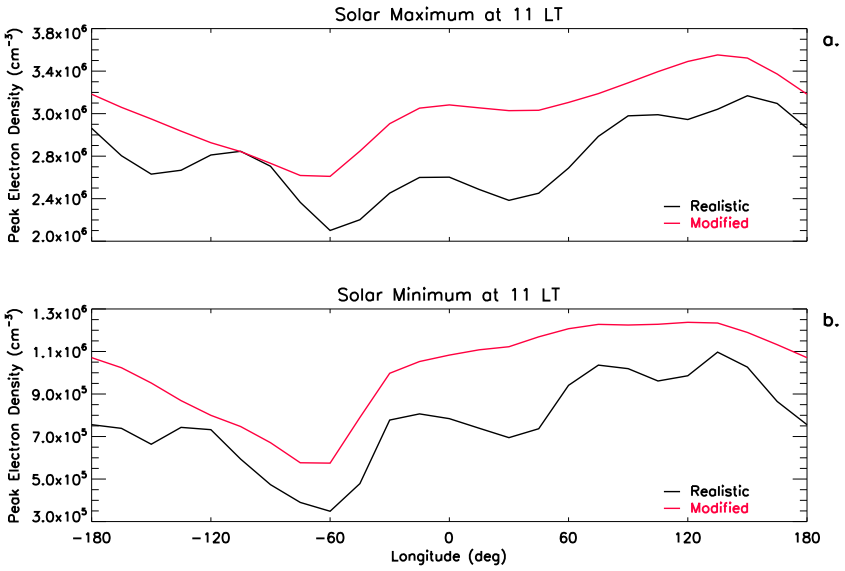

Figure 9. TIME-GCM peak electron density at 11 LT between 16.25° and 23.75° N under (a) solar maximum conditions and (b) solar minimum conditions. Realistic (modified) electron densities are represented by the black (red) lines.

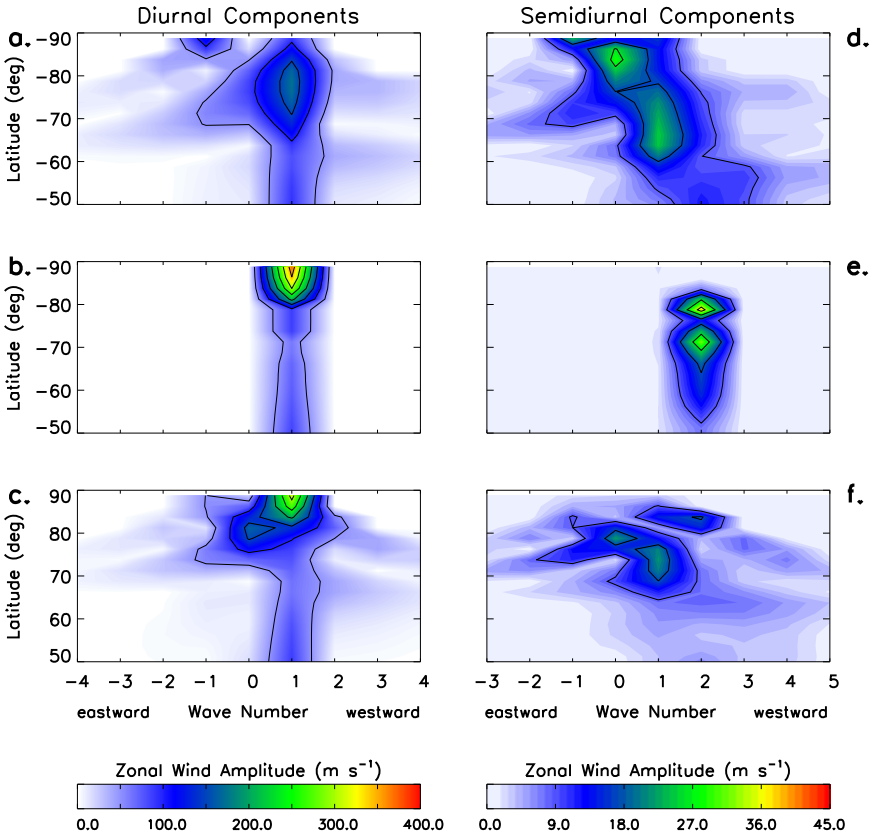

Figure 10. Zonal wind wave spectra of the diurnal and semidiurnal tidal components from the TIME-GCM at pressure level 3.5 (∼500 km), during September under solar maximum conditions; (a, d) modified flow results at high southern latitudes; (c, f) modified flow results at high northern latitudes; (b, e): idealized flow results at high southern latitudes. Diurnal (Semidiurnal) components are contoured every 50 (9) m s^{-1}, respectively.

spatial differences in the zonal winds between the modified and idealized circulations under solar maximum conditions at pressure level 3.5 (∼500 km) at (a) 2 LT, (b) 8 LT, (c) 14 LT, and (d) 20 LT. The largest zonal wind differences between the modified and idealized circulation occurs from 18 LT to 1 LT (not shown), and can be seen when comparing the differences shown in Figure 6d with Figures 6a, 6b, and 6c. Differences in zonal winds during these local times range from –110 to 140 m s^{-1} and are mainly attributed to differences in the ion drag term between the modified and idealized circulations. The sharp increase in the zonal wind difference at 18 LT coincides with the onset time of the pre-reversal enhancement (PRE), which is defined as a sharp increase in the vertical ion drift motion around sunset via an enhancement of the eastward electric field strength in the E-region. Since ion motions are organized relative to the Earth's magnetic field, a spatially variant ionosphere (i.e., modified case) will lead to spatially variant ion concentrations along these magnetic field lines. Thus, zonal wind differences between the modified and idealized circulations starting around dusk (∼18 LT) and persisting to around midnight (∼0 LT) are most likely driven by the PRE. Smaller zonal wind differences (–60 to 80 m s^{-1}) occur from 2 LT to 17 LT, and these smaller zonal wind differences are attributable to considerably smaller differences in both the ion drag and pressure gradient terms in the zonal momentum equation. Zonal wind differences at solar minimum (not shown) from 18 LT to 1 LT (2 LT to 17 LT) are smaller by a factor of ∼7 (∼2) when compared to solar maximum results. Throughout the entire day, meridional wind differences (not shown) are driven by a combination of the pressure gradient force differences and zonal momentum response differences. Between 18 LT to 1 LT at solar maximum, meridional wind differences are larger by a factor of ∼3 when compared with solar minimum meridional wind differences. However, from 2 LT to 17 LT, meridional wind differences are comparable between the solar maximum and solar minimum.

[23] It is important to note that temperature differences between the modified and idealized cases also exist, due to adiabatic heating and cooling differences. Adiabatic heating and cooling differences are a result of vertical wind differences between the modified and idealized cases. This is best illustrated at night, in the absence of solar heating. For example, Figure 7 compares difference fields of two terms in the thermodynamic energy equation at 3 LT with the temperature differences between the modified and idealized cases at 5 LT and ∼500 km at low and middle latitudes during solar maximum. Specifically, Figure 7a shows the adiabatic heating and cooling differences between the modified and idealized cases, while Figure 7b shows the differences of the time derivative of temperature between the modified and idealized cases. Similar spatial structures in the difference

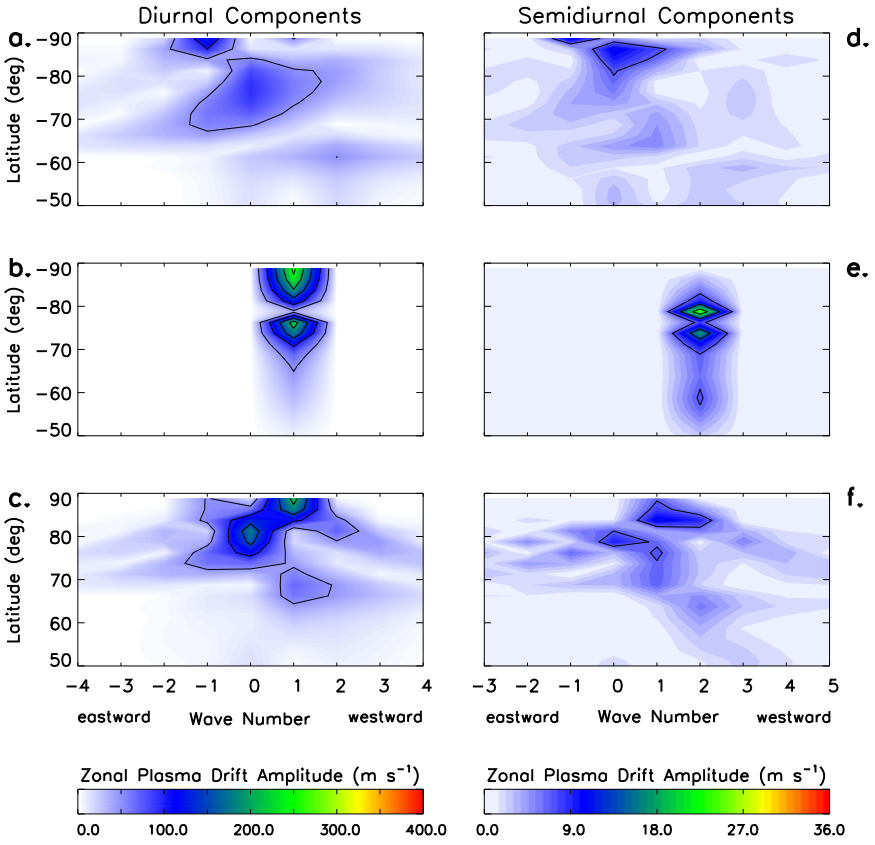

Figure 11. Same as Figure 10 except for the zonal plasma drift.

fields displayed in Figures 8a and 8b imply that the adiabatic heating and cooling term is the dominant term in the thermodynamic energy equation, thereby leading to the greatest changes in temperature with time. Further comparison between the difference fields of $\frac{\partial T}{\partial t}$ (Figure 7b) at 3 LT and the overall temperature differences shown in Figure 7c at 5 LT, reveals similar spatial features. We find an analogous result in Figure 8 during solar minimum conditions, leading us to conclude that adiabatic heating and cooling differences are ultimately responsible for low and middle latitude temperature differences between the modified and idealized circulations at night, independent of solar cycle condition. However, we note that at solar maximum, the temperature differences calculated are larger than those at solar minimum mainly due to larger ionization anomalies. Also, in order to completely replicate the time derivative of temperatures differences shown in Figures 8c and 9c we must consider other terms from the thermodynamic energy equation, including heat transfer by molecular diffusion, advection, and radiative cooling. At night, these terms are comparatively small when compared to the adiabatic heating and cooling term. However, during the daytime, these terms become non-negligible.

[24] Finally, we return to the question raised in section 2, as to whether the wave-4 signature in the neutral atmosphere at solar minimum (Figure 1g) could be produced by something other than the direct vertical penetration of DE3 and SE2. To further explore this possibility, consider Figure 9, which displays the September peak electron density from the modified and realistic TIME-GCM simulations at 11 LT between 16.25° and 23.75°N, for solar maximum and solar minimum conditions. The wave-4 signature that is evident at both levels of solar activity is likely due to electric fields driven by the E-region wind dynamo processes associated with DE3 [*Hagan et al.*, 2007]. Spectral analysis of the peak electron density shown in Figure 9 reveals that the wave-4 perturbation for solar maximum (Figure 9a, black line) is about 6% of the mean value with an absolute amplitude of 1.7×10^5 cm^{-3}, whereas at solar minimum (Figure 9b, black line) the relative perturbation is about 12% and has an absolute magnitude of 9.1×10^4 cm^{-3}. These wave-4 perturbation amplitudes in peak electron density are of similar order to those in latitudinally averaged TEC observations [*Wan et al.*, 2010] for solar medium (5%) and minimum (8%) conditions at 11 LT during September. Since the mean during solar maximum is about 3.5 times that at solar minimum, and the wave-4 absolute amplitude is twice as great, the wave-4 momentum source term at solar maximum is roughly seven times greater the wave-4 momentum source term at solar minimum, yet, the wave-4 signature in the neutral atmosphere at solar maximum is small (Figure 1c). From this we conclude that the wave-4 signature that is produced in the neutral atmosphere by any dynamo-related process at solar minimum is even smaller, and that the wave-4 seen in the neutral atmosphere in our simulations during solar minimum (Figure 1g) is overwhelmingly due to the direct vertical propagation by DE3 and SE2.

5. In Situ Generated Non-migrating Tides at High-Latitudes

[25] In this section, we extend our analysis to high-latitudes. At high-latitudes, the momentum source terms for the modified neutral circulation now take their full form from (3) and (4), i.e, $\epsilon(u - u^E)$ and $\epsilon(v - v^E)$, which is a result of rotating the idealized circulation into the new magnetic frame. Therefore, the momentum source terms that drive the neutral modified circulation arise from two sources: (a) the modified ion drag terms times the DW1 and SW2 of the idealized circulation (same as at low latitudes) and (b) the modified ion drag terms times the components of the plasma drift circulation in the new magnetic frame (i.e., not DW1 and SW2 from the idealized plasma circulation). As expected, Figures 10b and 10e show that the idealized circulations above 60° latitude in both hemispheres consist of DW1, SW2 and a zonal mean component (not shown), and from Figure 2 we see that the ion drag components at high latitudes primarily consist of the zonal mean, SPW1, D0, DW1 and SW2. Following the logic developed in Section 3, the corresponding momentum source terms for the modified circulation consist of the sum and difference products of ϵ and u. These include all of the components illustrated in Figures 10a, 10c, 10d, and 10f (i.e., DW1, D0, DE1, S0, and SW1) plus other smaller components including terdiurnal ones. Turning now to the spectra of zonal plasma drifts, (u^E) in Figure 11, we see that the modified plasma circulation also consists of DW1, D0, DE1, S0, and SW1. Since the zonal mean term of the ion drag is so large, the interaction between the modified ion drag and the plasma drift circulation in the new magnetic frame may be the dominant momentum source term for the high-latitude tidal components. However, we are not able to unambiguously separate the relative contributions of these forcing terms to the final modified circulation components depicted in Figure 10.

[26] Further comparison between non-migrating tidal components generated in situ at high southern latitudes with those at high northern latitudes reveals interhemispheric differences in both amplitude and latitudinal structure. The offset between the geomagnetic and geographic poles differs between hemispheres suggesting that the ion-neutral coupling processes and non-migrating tidal excitation, will differ in detail. We also note that the wave spectra shown in Figure 10 for the modified circulation closely resembles wave spectra from the realistic circulation under both solar maximum and solar minimum conditions (not shown), thereby suggesting these non-migrating tidal components are generated in situ, regardless of solar cycle.

[27] Similar to the analysis performed in Section 4, temperature differences between the modified and idealized cases also exist at high latitudes (not shown). However, we have not pursued the origins of these temperature differences in relation to momentum source terms since other effects (i.e., joule and particle heating) can also produce high-latitude temperature differences.

6. Summary and Conclusions

[28] The importance of migrating and non-migrating tides to the dynamics and electrodynamics of the IT system is widely recognized. In many cases these tides propagate and electrodynamically couple into the IT from sources in the troposphere, but recent observational evidence suggests the existence of non-migrating tides excited in situ as well. The present work demonstrates that non-migrating tidal components can be generated in situ in the upper thermosphere due to ion-neutral coupling. Using six different TIME-GCM simulations, we distinguish between diurnal and semidiurnal migrating and non-migrating tidal components generated locally in the thermosphere from those that originate in the troposphere. The prominent results and conclusions are as follows:

[29] 1. At low and middle latitudes, comparison between modified and idealized circulations reveals that migrating and non-migrating tides are generated in situ through ion-neutral interactions due to the longitude-dependent ionosphere imposed by the realistic magnetic field configuration.

[30] 2. During solar maximum, non-migrating diurnal and semidiurnal tides forced by ion-neutral interactions are responsible for the majority of the longitude-dependent tidal structure seen in the low and middle latitude upper thermosphere. More specifically, non-migrating tidal components D0 and DW2 arising from hydromagnetic coupling between SPW1 (modified ionosphere) and DW1 (idealized wind circulation) reach amplitudes of up to 20 m s^{-1} at ∼500 km. Also, DE1 exists due to hydromagnetic coupling between SPW2 (modified ionosphere) and DW1 (idealized wind circulation), reaching amplitudes of up to ∼15 m s^{-1} at ∼500 km. Smaller amplitude (i.e., ranging from 1–10 m s^{-1}) semidiurnal non-migrating tidal components including SE1, S0, SW1, and SW3 are also present at ∼500 km. These tides are a result of hydromagnetic coupling between SW2 and SPW3, SPW2, and SPW1, respectively. The above results are in accord with the tidal observations from CHAMP shown in *Häusler and Lühr* [2009] and *Häusler et al.* [2010].

[31] 3. Since DE3 and SE2 are the two largest amplitude non-migrating tides at ∼350 km under solar minimum conditions and a wave-4 longitude variation in temperature and winds exists, we conclude that tropospherically forced tides dominate the tidal spectrum in the upper thermosphere at low and middle latitudes during solar minimum. The aforementioned wave-4 variation in temperature and winds at ∼350 km under solar minimum conditions are consistent with the direct penetration of the DE3 and SE2 into the F-region ionosphere, due to reduced dissipation in the IT during solar minimum as concluded by *Oberheide et al.* [2009]. Neutral wind dynamo effects of these same tidal components produce a wave-4 signature in the ionosphere that compares reasonably well with the observations present in Figure 4 of *Wan et al.* [2010]. However, these effects do not play a significant role in driving the wave-4 variation in temperature and winds calculated in the TIME-GCM at ∼350 km under solar minimum conditions.

[32] 4. The aggregate effect of these non-migrating tides generated due to ion-neutral interactions at low and middle latitudes under solar maximum conditions are relatively large with extrema ranging from –110 to 140 m s^{-1} in latitude versus longitude local time snapshots. However, at solar minimum the aggregate effects at low and middle latitudes are much smaller with extrema ranging from 10 to 40 m s^{-1}.

[33] 5. Longitudinal temperature differences associated with the modified and idealized flows exist due to vertical

winds accompanying the modified circulation which lead to adiabatic heating and cooling differences at night time. However, during the day, other terms in the thermodynamic energy equation become as important as adiabatic heating and cooling. Large ionization anomalies during solar maximum lead to larger temperature differences between the modified and idealized cases. These temperature differences can range from –40 to 50 K at low to middle latitudes during the late evening when viewed from a latitude versus longitude constant local time perspective.

[34] 6. High-latitude in situ generated migrating and non-migrating tides driven by combined hydromagnetic coupling and convection electric field effects exhibit interhemispheric differences in both amplitude and latitude structure due to interhemispheric differences between the offset of the geographic and geomagnetic poles. Non-migrating tidal components include DE1, D0, DW2, SW1, S0, and SE1. These non-migrating tidal components are seen in both the modified and realistic circulations during both solar minimum and solar maximum. We, therefore, conclude that the majority of non-migrating tidal components observed at high latitudes are generated locally in the thermosphere.

[35] **Acknowledgments.** Discussions with Nick Pedatella, Xiaoli Zhang, and Arthur Richmond regarding atmospheric tides in a local time perspective and aligned dipole magnetic field dynamics were much appreciated. This work was supported under Grant ATM-0903179 from the National Science Foundation to the University of Colorado. The National Center for Atmospheric Research is sponsored by the National Science Foundation.

[36] Robert Lysak thanks the reviewers for their assistance in evaluating this paper.

References

Angelats i Coll, M., and J. M. Forbes (2002), Nonlinear interactions in the upper atmosphere: The $s = 1$ and $s = 3$ non-migrating semidiurnal tides, *J. Geophys. Res.*, *107*(A8), 1157, doi:10.1029/2001JA900179.

Chapman, S., and R. S. Lindzen (1970), *Atmospheric Tides: Thermal and Gravitational*, 200 pp, Gordon and Breach, New York.

Dickinson, R. E., and R. G. Roble (1972), Thermospheric motion and temperature perturbations from global-scale winds flowing through F region ionization anomalies, *Space Res.*, *12*, 1079–1085.

England, S. L., X. Zhang, T. J. Immel, J. Forbes, and R. DeMajistre (2009), The effect of non-migrating tides on the morphology of the equatorial ionospheric anomaly: Seasonal variability, *Earth Planets Space*, *61*, 493–503.

England, S. L., T. J. Immel, J. D. Huba, M. E. Hagan, A. Maute, and R. DeMajistre (2010), Modeling of multiple effects of atmospheric tides on the ionosphere: An examination of possible coupling mechanisms responsible for the longitudinal structure of the equatorial ionosphere, *J. Geophys. Res.*, *115*, A05308, doi:10.1029/2009JA014894.

Evans, D. S. (1987), Global statistical patterns of auroral phenomena, in *Proceedings of the Symposium on Quantitative Modeling of Magnetospheric-Ionospheric Coupling Processes*, edited by Y. Kamide and R. A. Wolf, pp. 325–330, Kyoto Sangyo University, Kyoto, Japan.

Forbes, J. M. (1982), Atmospheric Tides, 1, Model description and results for the solar diurnal component, *J. Geophys. Res.*, *87*(A7), 5222–5240, doi:10.1029/JA087iA07p05222.

Forbes, J. M., and H. B. Garrett (1979), Theoretical studies of atmospheric tides, *Rev. Geophys.*, *17*, 1951–1981.

Forbes, J. M., M. E. Hagan, X. Zhang, and K. Hamilton (1997), Upper atmospheric tidal oscillations due to latent heat release in the tropical troposphere, *Ann. Geophys.*, *15*, 1165–1175.

Forbes, J. M., J. Russell, S. Miyahara, X. Zhang, S. Palo, M. Mlynczak, C. J. Mertens, and M. E. Hagan (2006), Troposphere-thermosphere tidal coupling as measured by the SABER instrument on TIMED during July–September 2002, *J. Geophys. Res.*, *111*, A10S06, doi:10.1029/2005JA011492.

Forbes, J. M., X. Zhang, S. Palo, J. Russell, C. J. Mertens, and M. Mlynczak (2008), Tidal variability in the ionospheric dynamo region, *J. Geophys. Res.*, *113*, A02310, doi:10.1029/2007JA012737.

Forbes, J. M., S. L. Bruinsma, X. Zhang, and J. Oberheide (2009), Surface-exosphere coupling due to thermal tides, *Geophys. Res. Lett.*, *36*, L15812, doi:10.1029/2009GL038748.

Hagan, M. E. (1996), Comparative effects of migrating solar sources on tidal signatures in the middle and upper atmosphere, *J. Geophys. Res.*, *101*(D16), 21,213–21,222, doi:10.1029/96JD01374.

Hagan, M. E., and J. M. Forbes (2002), Migrating and non-migrating diurnal tides in the middle and upper atmosphere excited by tropospheric latent heat release, *J. Geophys. Res.*, *107*(D24), 4754, doi:10.1029/2001JD001236.

Hagan, M. E., and J. M. Forbes (2003), Migrating and non-migrating semidiurnal tides in the upper atmosphere excited by tropospheric latent heat release, *J. Geophys. Res.*, *108*(A2), 1062, doi:10.1029/2002JA009466.

Hagan, M. E., J. M. Forbes, and F. Vial (1995), On modeling migrating solar tides, *Geophys. Res. Lett.*, *22*, 893–896.

Hagan, M. E., M. D. Burrage, J. M. Forbes, J. Hackney, W. J. Randel, and X. Zhang (1999), GSWM-98: Results for migrating solar tides, *J. Geophys. Res.*, *104*(A4), 6813–6827.

Hagan, M. E., R. G. Roble, and J. Hackney (2001), Migrating thermospheric tides, *J. Geophys. Res.*, *106* (A7), 12,739–12,752, doi:10.1029/2000JA000344.

Hagan, M. E., A. Maute, R. G. Roble, A. D. Richmond, T. J. Immel, and S. L. England (2007), Connections between deep tropical clouds and the Earth's ionosphere, *Geophys. Res. Lett.*, *34*, L20109, doi:10.1029/2007GL030142.

Hagan, M. E., A. Maute, and R. G. Roble (2009), Tropospheric tidal effects on the middle and upper atmosphere, *J. Geophys. Res.*, *114*, A01302, doi:10.1029/2008JA013637.

Häusler, K., and H. Lühr (2009), Nonmigrating tidal signals in the upper thermospheric zonal wind at equatorial latitudes as observed by CHAMP, *Ann. Geophys.*, *27*, 2643–2652.

Häusler, K., H. Lühr, M. E. Hagan, A. Maute, and R. G. Roble (2010), Comparison of CHAMP and TIME-GCM non-migrating tidal signals in the thermospheric zonal wind, *J. Geophys. Res.*, *115*, D00108, doi:10.1029/2009JD012394.

Immel, T. J., E. Sagawa, S. L. England, S. B. Henderson, M. E. Hagan, S. B. Mende, H. U. Frey, C. M. Swenson, and L. J. Paxton (2006), Control of equatorial ionospheric morphology by atmospheric tides, *Geophys. Res. Lett.*, *33*, L15108, doi:10.1029/2006GL026161.

Jin, H., Y. Miyoshi, H. Fujiwara, and H. Shinagawa (2008), Electrodynamics of the formation of ionospheric wave number 4 longitudinal structure, *J. Geophys. Res.*, *113*, A09307, doi:10.1029/2008JA013301.

Kil, H., S.-J. Oh, M. C. Kelley, L. J. Paxton, S. L. England, E. Talaat, K.-W. Min, and S.-Y. Su (2007), Longitudinal structure of the vertical E × B drift and ion density seen from ROCSAT-1, *Geophys. Res. Lett.*, *34*, L14110, doi:10.1029/2007GL030018.

Lin, C. H., W. Wang, M. E. Hagan, C. C. Hsiao, T. J. Immel, M. L. Hsu, J. Y. Liu, L. J. Paxton, T. W. Fang, and C. H. Liu (2007), Plausible effect of atmospheric tides on the equatorial ionosphere observed by the FORMOSAT-3/COSMIC: Three-dimensional electron density structures, *Geophys. Res. Lett.*, *34*, L11112, doi:10.1029/2007GL029265.

Lindzen, R. S. (1978), Effect of daily variations of cumulonimbus activity on the atmospheric semidiurnal tide, *Mon. Weather Rev.*, *106*, 526–533.

Liu, H., and S. Watanabe (2008), Seasonal variation of the longitudinal structure of the equatorial ionosphere: Does it reflect tidal influences from below? *J. Geophys. Res.*, *113*, A08315, doi:10.1029/2008JA013027.

Lühr, H., K. Häusler, and C. Stolle (2007), Longitudinal variation of F region electron density and thermospheric zonal wind caused by atmospheric tides, *Geophys. Res. Lett.*, *34*, L16102, doi:10.1029/2007GL030639.

Lühr, H., M. Rother, K. Häusler, P. Alken, and S. Maus (2008), The influence of nonmigrating tides on the longitudinal variation of the equatorial electrojet, *J. Geophys. Res.*, *113*, A08313, doi:10.1029/2008JA013064.

Lühr, H., M. Rother, K. Häusler, B. Fejer, and P. Alken (2012), Direct comparison of non-migrating tidal signatures in the electrojet, vertical plasma drift and equatorial ionization anomaly, *J. Atmos. Sol. Terr. Phys.*, *73*, 31–43, doi:10.1016/j.jastp.2011.07.009.

Mayr, H. G., J. G. Mengel, E. R. Talaat, H. S. Porter, and K. L. Chan (2003), Non-migrating diurnal tides generated with planetary waves in the Mesosphere, *Geophys. Res. Lett.*, *30*(16), 1832, doi:10.1029/2003GL017877.

McLandress, C. (2001), The seasonal variation of the propagating diurnal tide in the mesosphere and lower thermosphere. Part I: The role of gravity waves and planetary waves, *J. Atmos. Sci.*, *59*, 893–906.

McLandress, C., and W. E. Ward (1994), Tidal/gravity wave interactions and their influence on the large-scale dynamics of the middle atmosphere: Model results, *J. Geophys. Res.*, *99*(D4), 8139–8155, doi:10.1029/94JD00486.

Oberheide, J., and J. M. Forbes (2008), Tidal propagation of deep tropical cloud signatures into the thermosphere from TIMED observations, *Geophys. Res. Lett.*, *35*, L04816, doi:10.1029/2007GL032397.

Oberheide, J., M. E. Hagan, R. G. Roble, and D. Offermann (2002), Sources of non-migrating tides in the tropical middle atmosphere, *J. Geophys. Res.*, *107*(D21), 4567, doi:10.1029/2002JD002220.

Oberheide, J., J. M. Forbes, K. Häusler, Q. Wu, and S. L. Bruinsma (2009), Tropospheric tides from 80 to 400 km: Propagation, interannual variability, and solar cycle effects, *J. Geophys. Res.*, *114*, D00I05, doi: 10.1029/2009JD012388.

Oberheide, J., J. M. Forbes, X. Zhang, and S. L. Bruinsma (2011a), Wave-driven variability in the ionosphere-thermosphere-mesosphere system from TIMED observations: What contributes to the wave 4? *J. Geophys. Res.*, *116*, A01306, doi:10.1029/2010JA015911.

Oberheide, J., J. M. Forbes, X. Zhang, and S. L. Bruinsma (2011b), Climatology of upward propagating diurnal and semidiurnal tides in the thermosphere, *J. Geophys. Res.*, *116*, A11306, doi:10.1029/2011JA016784.

Pancheva, D., and P. Mukhtarov (2010), Strong evidence for the tidal control on the longitudinal structure of the ionospheric F-region, *Geophys. Res. Lett.*, *37*, L14105, doi:10.1029/2010GL044039.

Pedatella, N. M., J. M. Forbes, A. Maute, A. D. Richmond, T.-W. Fang, K. M. Larson, and G. Millward (2011), Longitudinal variations in the F region ionosphere and the topside ionosphere-plasmasphere: Observations and model simulations, *J. Geophys. Res.*, *116*, A12309, doi: 10.1029/2011JA016600.

Pedatella, N. M., M. E. Hagan, and A. Maute (2012), The comparative importance of DE3, SE2, and SPW4 on the generation of wavenumber-4 longitude structures in the low-latitude ionosphere during September equinox, *Geophys. Res. Lett.*, *39*, L19108, doi:10.1029/2012GL053643.

Richmond, A. D. (1970), Geomagnetic crochets and ionospheric tidal winds, Ph. D. thesis, University of Californis, Los Angeles.

Richmond, A. D. (1971), Tidal winds at ionospheric heights, *Radio Sci.*, *6*, 175–189.

Roble, R. G. (1995), Energetics of the mesosphere and thermosphere, in *The Upper Mesosphere and Lower Thermosphere: A Review of Experiment and Theory, Geophysical Monographs Series*, vol. 87, edited by R. M. Johnson and T. L. Killeen, pp. 121, AGU, Washington, D. C.

Roble, R. G. (1996), The NCAR thermosphere-ionosphere-mesosphere-electrodynamics general circulation model (TIME-GCM), in *STEP Handbook on Ionospheric Models*, edited by R. W. Schunk, pp. 281–288, Utah State University, Logan.

Roble, R. G., and R. E. Dickinson (1974), The effect of displaced geomagnetic and geographic poles on the thermospheric neutral winds, *Planet. Space Sci.*, *22*, 623–631.

Roble, R. G., and E. C. Ridley (1994), A thermosphere-ionosphere-mesosphere-electrodynamics general circulation model (TIME-GCM): Equinox solar cycle minimum simulations (30–500 km), *Geophys. Res. Lett.*, *21*(6), 417–420, doi:10.1029/93GL03391.

Sagawa, E., T. J. Immel, H. U. Frey, and S. B. Mende (2005), Longitudinal structure of the equatorial anomaly in the nighttime ionosphere observed by IMAGE/FUV, *J. Geophys. Res.*, *110*, A11302, doi: 10.1029/2004JA010848.

Scherliess, L., D. C. Thompson, and R. W. Schunk (2008), Longitudinal variability of low-latitude total electron content: Tidal influences, *J. Geophys. Res.*, *113*, A01311, doi:10.1029/2007JA012480.

Teitelbaum, H., and F. Vial (1991), On tidal variability induced by nonlinear interaction with planetary waves, *J. Geophys. Res.*, *96*(A8), 14,169-14,178, doi:10.1029/91JA01019.

Teitelbaum, H., F. Vial, A. H. Manson, R. Giraldez, and M. Massebeuf (1989), The diurnal and semidiurnal tides: Terdiurnal and diurnal secondary waves, *J. Atrnos. Terr. Phys.*, *51*, 627–634.

Vial, F., J. M. Forbes, and S. Miyahara (1991), Some transient aspects of tidal propagation, *J. Geophys. Res.*, *96*(A2), 1215–1224, doi: 10.1029/90JA02181.

Walterscheid, R. L., G. G. Sivjee, G. Schuberatnd, and R. M. Hamwey (1986), Large amplitude semi-diurnal variations in the polar mesopause: Evidence of a pseudotide, *Nature*, *324*, 347.

Wan, W., J. Xiong, Z. Ren, L. Liu, M.-L. Zhang, F. Ding, B. Ning, B. Zhao, and X. Yue (2010), Correlation between the ionospheric WN4 signature and the upper atmospheric DE3 tide, *J. Geophys. Res.*, *115*, A11303, doi: 10.1029/2010JA015527.

Zhang, X., J. M. Forbes, and M. E. Hagan (2010a), Longitudinal variation of tides in the MLT region: 1. Tides driven by tropospheric net radiative heating, *J. Geophys. Res.*, *115*, A06316, doi:10.1029/2009JA014897.

Zhang, X., J. M. Forbes, and M. E. Hagan (2010b), Longitudinal variation of tides in the MLT region: 2. Relative effects of solar radiative and latent heating, *J. Geophys. Res.*, *115*, A06317, doi:10.1029/2009JA014898.